Diffusional Channeling in the Sulfate-Activating Complex: Combined Continuum Modeling and Coarse-Grained Brownian Dynamics Studies

Yuhui Cheng,*† Chia-en A. Chang,¶ Zeyun Yu,‡ Yongjie Zhang,‖ Meihao Sun,** Thomas S. Leyh,** Michael J. Holst,‡ and J. Andrew McCammon*†§

*Howard Hughes Medical Institute, †Department of Chemistry and Biochemistry, and Center for Theoretical Biological Physics, ‡Department of Mathematics, and §Department of Pharmacology, University of California at San Diego, La Jolla, California; ¶Department of Chemistry, University of California at Riverside, Riverside, California; ‖Department of Mechanical Engineering, Carnegie Mellon University, Pittsburgh, Pennsylvania; and **Department of Biochemistry, Albert Einstein College of Medicine, Bronx, New York

ABSTRACT Enzymes required for sulfur metabolism have been suggested to gain efficiency by restricted diffusion (i.e., channeling) of an intermediate APS^{2-} between active sites. This article describes modeling of the whole channeling process by numerical solution of the Smoluchowski diffusion equation, as well as by coarse-grained Brownian dynamics. The results suggest that electrostatics plays an essential role in the APS^{2-} channeling. Furthermore, with coarse-grained Brownian dynamics, the substrate channeling process has been studied with reactions in multiple active sites. Our simulations provide a bridge for numerical modeling with Brownian dynamics to simulate the complicated reaction and diffusion and raise important questions relating to the electrostatically mediated substrate channeling in vitro, in situ, and in vivo.

INTRODUCTION

Channeling is a process by which a reaction intermediate (I) from the active site of one enzyme (E1) is transported directly to the active site of a second enzyme (E2) rather than being dissociated into the bulk phase. Channeling of this kind can theoretically occur within multifunctional enzymes, tightly associated multienzyme complexes, or transient enzyme complexes (1,2). Substrate channeling has many advantages over the free diffusion of reaction intermediates through the bulk solvent:

Isolating intermediates from competing reactions (3).
Circumventing unfavorable equilibria and kinetics imposed by bulk phase metabolite concentrations (4).
Protecting unstable intermediates (5).
Conserving the scarce solvation capacity of the cell (6).
Enhancing catalysis by avoiding unfavorable energetics of desolvating substrates (7).
Reducing lag transients (times to reach steady-state response to a change in substrate concentration upstream in a coupled reaction path) (8).
Providing new means of metabolic regulation by modulation of enzyme associations, and increased sensitivities to regulatory signals (9).

Numerous examples of substrate channeling have been reported, including DNA replication, RNA synthesis, purine and pyrimidine biosynthesis, protein biosynthesis, amino-acid metabolism, lipid metabolism, glycolysis, and the tricarboxylic acid cycle, etc. (10–13). Up to now, two different mechanisms of channeling of the reaction intermediate have been proposed:

1. Tunneling of reaction intermediates within the protein matrix, such as NH_3 transferring in *Escherichia coli* carbamoyl-phosphate synthetase (13).
2. Electrostatic channeling of reaction intermediates across the protein surface, such as $H_2folate^{2-}$ transfer in *Leishmania major* dihydrofolate reductase-thymidylate synthase (DHFR-TS) (14).

Considering the significance of substrate channeling and the uncertainties of the experimental studies, computational study of the channeling process should be helpful. In principle, computational studies can provide detailed information and insights to complement experimental studies. However, this goal can only be attained when appropriate computational approaches are employed and the system studied is a good mimic of the multifunctional enzyme system. Previously Brownian dynamics has been successfully applied on several other channeling proteins by Elcock et al., such as channeling of the $-2e$ charged intermediate across the molecular surface of the DHFR-TS complexes (15), and oxaloacetate channeling from the active site of the malate dehydrogenase to the active site of the citrate synthase (3,16). Recently, several molecular dynamics studies on ammonia channeling in the protein matrix have been reported, revealing an open-gate mechanism proposed by Amaro and

Submitted June 13, 2008, and accepted for publication July 22, 2008.

Address reprint requests to Yuhui Cheng, Tel.: 858-822-2771; E-mail: ycheng@mcammon.ucsd.edu.

Editor: Steven D. Schwartz.

0006-3495/08/11/4659/09 $2.00

doi: 10.1529/biophysj.108.140038

Luthey-Schulten (17) and roles of key residues in bacterial glucosamine-6-phosphate synthase by Floquet et al. (18).

Sulfate-activating complexes (SACs), essential to life for metabolic assimilation of sulfur, have been suggested to utilize channeling. *Homo sapiens* (type I), *Mycobacterium tuberculosis* (type II), and *Rhodobacter sphaeroides* (type III) represent three typical SACs (19,20). As shown in Fig. 1, there are four active sites in the type III SAC dimer (only two have been labeled in color). The intermediate APS^{2-} is synthesized in the active site of ATP sulfurylase (labeled in *yellow*), which transfers the adenylyl moiety of ATP from pyrophosphate to sulfate to form adenosine 5′-phosphosulfate (APS) (reaction 1). The second active site, labeled in red, phosphorylates APS at the 3′-hydroxyl of the ribose ring to produce 3′-phosphoadenosine 5′-phosphosulfate (PAPS) (reaction 2). Between the two active sites, there is a 75-Å-long channel that interconnects active-site pairs:

$$ATP^{4-} + SO_4^{2-} \xrightarrow{k_{cat}/K_m} APS^{2-} + P_2O_7^{4-}, \quad (1)$$

$$ATP^{4-} + APS^{2-} \xrightarrow{k'_{cat}/K'_m} ADP^{3-} + PAPS^{4-} + H^+. \quad (2)$$

The intermediate APS^{2-} synthesized by the active site of ATP sulfurylase has two possible pathways: one is to diffuse into the solvent and be reduced by APS reductase; the other is to diffuse into the APS kinase active site and be phosphorylated. The channeling titration assays have demonstrated that the channeling efficiency of the type III complex is quite high and larger than 95% (19,20).

In this work, we apply our SMOL program to solve the steady-state and time-dependent Smoluchowski equation for the APS channeling process (21). The release and phosphorylation of APS^{2-} have been coupled by specifying reactive boundaries for the APS^{2-} channeling. By modifying the charge on the APS^{2-} ion, we have found that electrostatic steering is essential for this substrate channeling case. Nearly 99% of APS^{2-} is delivered to the active site of the APS kinase via channeling, while >30% of APS^{2-} leaks into the solvent if the APS intermediate is neutral. Furthermore, we have directly observed the APS steady-state distribution with the numerical calculations, as well as the APS dynamics along the channel via the coarse-grained Brownian dynamics. Our simulation results corroborated the experimental result and show that the channeling in the type III SAC is via an electrostatic highway crossing the enzyme surface to connect different catalytic centers. The combined continuum simulation and Brownian dynamics provide clear prototypes for modeling complicated reaction-diffusion systems.

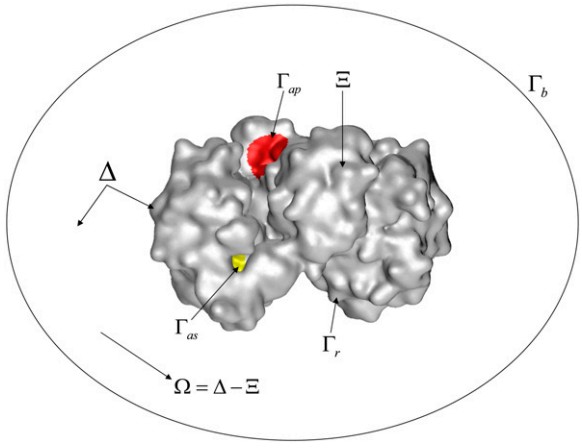

FIGURE 1 Two active sites in the type III SAC dimer and boundary information. The values Ξ and Δ represent the SAC domain and whole spherical domain, respectively. The value $\Omega = \Delta - \Xi$ represents the diffusion domain. The active site of ATP sulfurylase is in yellow and that of APS kinase is in red. The values Γ_b and Γ_r represent the reflective Neumann boundary, while the two active sites Γ_{as} and Γ_{ap} are reactive Robin boundaries.

MATERIALS AND METHODS

The structure of the type III SAC dimer used here was homology-modeled with the SWISS-MODEL program, as described previously (20). The structural models reveal a 75 Å-long channel that interconnects active-site pairs in the complex and that opens and closes in response to occupancy of those sites. The T-state, which corresponds to the open state, has been studied in this article.

Electrostatic potential calculations

The electrostatic potentials in the diffusion domain were obtained by solving the Poisson-Boltzmann equation. APBS 0.5.1 is used to calculate the potentials, which correspond to the potential input $W(r)$ in the time-dependent Smoluchowski equation (22–24). The partial charges and radii of each atom in the sulfate activating complex have been assigned using the AMBER99 force field, and the dielectric constant is set as 4.0 inside the protein and 78.0 for the solvent. The solvent probe radius is set as 1.4 Å, and the ion exclusion layer is set as 2.0 Å. Since the reaction mixture in the experiment contains SAC (19 nM), ATP (2.0 mM), SO_4^{2-} (6.0 mM), and $MgCl_2$ (4.0 mM), the ionic strength has been set at 0.040 M in our simulations. The concentrations of ATP, SO_4^{2-}, and $MgCl_2$ are far higher than that of the SAC, and the concentration of the released APS^{2-} should be relatively low, therefore, the ionic strength is approximately constant (20). As in several previous studies (21,25,26), the diffusion boundary has been set at 20 times the radius of the biomolecule. The electrostatic potential on the boundary is approximated as zero. A series of nested potential grids is constructed in a multiresolution format where higher resolution meshes provide potential values near the molecular surface while coarser meshes are used away from the molecule. The dimensions of the finest grid are given by the psize.py utility in the APBS software package, and the coarsest grid dimensions are set to cover the whole problem domain plus two grid spacings (to allow gradient calculation) in each dimension. The setup for the rest of the grid hierarchy is calculated using a geometric sequence for grid spacing. For the SAC, the finest grid has dimensions of 125.0 Å × 107.3 Å × 110.3 Å with 225, 193, and 193 grid points in each direction, respectively. This corresponds to a 0.56 Å × 0.56 Å × 0.57 Å grid spacing setup.

Adaptive finite element mesh generation

The adaptive tetrahedral meshes were obtained and refined from the inflated van der Waals-based accessibility data for the complex dimer using the GAMer software (http://www./fetk.org/gamer) (27). GAMer, recently developed by Yu et al. (27), is an excellent adaptive finite element mesh tool,

which can generate very fine meshes near the active sites, and then label them as active. For this complex, there are two types of active sites:

1. The active site of ATP sulfurylase, in which APS^{2-} is generated.
2. The active site of APS kinase, in which APS^{2-} is phosphorylated.

Reactive Robin boundaries were defined on these active sites (21,25, 26,28).

The region between the biomolecule and a slightly larger sphere centered about the molecular center-of-mass was discretized initially by adaptive tetrahedral meshes. Very fine triangular elements were generated near the active site gorge, and coarser elements everywhere else. The mesh was then extended to the entire diffusion domain and the inside of the biomolecule with spatial adaptivity in that the mesh element size increases with increasing distance from the biomolecule.

The diffusion of APS^{2-} was modeled as that of a sphere with an exclusion radius of 8.0 Å and the diffusion coefficient of 1.5×10^3 Å$^2/\mu$s, which is similar to the diffusion coefficient of ATP^{4-} in cytoplasm (29).

The Smoluchowski equation with reaction-determined boundaries

To study the APS^{2-} channeling, we have simulated the SAC dimer with the time-dependent SMOL solver (http://mccammon.ucsd.edu/smol) (30). The time-dependent Smoluchowski equation has the form of a continuity equation,

$$\begin{aligned} -\nabla \cdot (a(\vec{R};t)\nabla u(\vec{R};t)) + \frac{\partial p(\vec{R};t)}{\partial t} &= 0 \quad \text{in} \quad \Omega, \\ \hat{n} \cdot a(\vec{R};t)\nabla p(\vec{R};t) &= k_1 \quad \text{for} \quad \vec{R} \in \Gamma_{as}, \\ p(\vec{R};t) &= 0.0 \quad \text{for} \quad \vec{R} \in \Gamma_{ap}, \\ \hat{n} \cdot \nabla p(\vec{R};t) &= 0 \quad \text{for} \quad \vec{R} \in \Gamma_{r}, \end{aligned} \tag{3}$$

where $a(\vec{R};t) = D(\vec{R})e^{-\beta W(\vec{R})}$ and $u(\vec{R};t) = e^{\beta W(\vec{R})}p(\vec{R};t)$.

Here $\hat{n}$ is the normal vector of the boundary and k_1 is the kinetic coefficient for the active site of the ATP sulfurylase Γ_{as}, while Γ_{ap} and Γ_r represent the active sites of the APS kinase and nonreactive molecular surface. The value $p(\vec{R};t)$ is the distribution function of the ensemble of Brownian particles, $D(\vec{R})$ is the diffusion coefficient, $\beta = 1/k_BT$ is the inverse Boltzmann energy, k_B is the Boltzmann constant, T is the temperature, and $W(\vec{R})$ is the potential of mean force for a diffusing particle due to solvent-mediated interactions with the target molecule. For simplicity, $D(\vec{R})$ can be assumed to be constant at 1.5×10^3 Å$^2/\mu$s.

According to Table 1, for the APS synthesis in the active site of ATP sulfurylase, $k_{cat}/K_m(ATP) \sim 10^4$ M^{-1} s^{-1}. The reaction is not diffusion-controlled. The concentration of the SACs is far lower than that of ATP or SO_4^{2-}, and the latter concentrations are substantially greater than the corresponding K_m values; therefore, the synthesis of APS^{2-} can be modeled as a zero-order reaction.

Similarly to how we have simulated reactions in the neuromuscular junction (21), we can define the APS^{2-} current out of the active site as

$$I([APS];t) := \int_{\Gamma_{as}} \hat{n} \cdot a(\vec{R};t)\nabla p(\vec{R};t)dS. \tag{4}$$

Here Γ_{as} denotes the surface of the active site of ATP sulfurylase. The quantity $j(\vec{R};t) = \hat{n} \cdot a(\vec{R};t)\nabla p(\vec{R};t)$ can be interpreted as the flux of APS molecules that are synthesized by the enzyme.

Finally, the reactive boundary in the active site of ATP sulfurylase can be depicted as

$$\frac{\partial [APS]}{\partial t} = \frac{k_{cat}[SAC]_{tot}}{1 + K_m/[S]} - I([APS];t). \tag{5}$$

TABLE 1 Type III sulfate-activating complex initial-rate parameters

ATP sulfurylase	
$K_m(\mu M)$ for ATP	150(30)
$K_m(\mu M)$ for SO_4	1000(70)
$k_{cat}(min^{-1})$	80(2)
APS kinase	
$K_m(\mu M)$ for ATP	24(0.7)
$K_m(\mu M)$ for APS	0.3(0.01)
$k_{cat}(min^{-1})$	260(4)

Because $[SO_4^{2-}] >$ [ATP], $K_m(ATP) = 0.150$ mM (Table 1), and [S] = 2.0 mM, then

$$\frac{K_m}{[S]} = \frac{0.150}{2.0} = 0.075.$$

When the steady state is achieved, $(d[APS]/dt) = 0$, i.e.,

$$\hat{n} \cdot a(\vec{R};t)\nabla p(\vec{R};t) = k'_{act,APS}k_{cat}[SAC]_{tot} = k_1. \tag{6}$$

Here $k'_{act,APS}$ is defined as the APS reaction coefficient, which can be determined by trial-and-error sampling.

For the phosphorylation reaction in APS kinase active site, the $k_{cat}/K_m(APS)$ reaches nearly 10^9 M^{-1} min^{-1}. Therefore, the reactive boundary can be described as the reactive Dirichlet, i.e., [APS] = 0.0.

Coarse-grained Brownian dynamics simulations

The Brownian dynamics simulation algorithm, together with a coarse-grained model (CGBD), was used to study the motions of the APS molecules in a discrete representation; this is complementary to the continuum representation. The CGBD simulation method is described in several publications (31,32). In this model, the amino acids are represented by one bead placed at the C_α of each residue (33). Each amino acid is assigned an effective radius (34), and $\pm 1e$ charge is assigned to a charged residue. For APS^{2-}, each adenine, ribose, and phosphosulfate group is represented by one bead, and $-1e$ is assigned to the latter two beads. An effective radius of each bead is assigned based on the size of each functional group, which is 3.0 Å, 2.5 Å, and 2.5 Å for adenine, ribose, and phosphosulfate groups, respectively. Since the system has $-22e$ net charge, we randomly distributed 22 Na^+ ions around the protein. The protein is held rigid, and the motion of each bead of APS is simulated with the BD algorithm of Ermak and McCammon (35) and Shen et al. (36). Although the slower protein fluctuations might play the role in the channeling process, the effect of conformational changes of the protein was not taken into account in this study (37,38). The diffusion coefficient used in the algorithm to move a bead was computed by the Stokes-Einstein equation, and the viscosity of water was set to 1 cp (T = 293 K).

In our coarse-grained model, the beads of APS are linked by virtual bonds and a bond angle; Coulombic and van der Waals interactions are applied for intermolecular interactions (31–33). A Lennard-Jones type functional form is used for van der Waals interactions, $U_{vdw} = 0.5[((r_i+r_j)/(r_{ij}))^8 - 1.5((r_i+r_j)/(r_{ij}))^6]$, where r_i and r_j are the effective radii of beads i and j, respectively. The Coulombic interaction is approximated by $U_{elec} = (q_iq_j/\varepsilon_{ij}r_{ij})$, and a distance-dependent dielectric coefficient ($\varepsilon_{ij} = 4r_{ij}$) is employed to avoid unrealistic in vacuo Coulombic interactions (39,40). APS^{2-} was placed in the first active site and a brief BD run was performed to allow APS^{2-} to move around the active site. The collected snapshots were used to initiate multiple BD runs to study binding pathways of APS^{2-} as it approached the active site of APS kinase. The simulations used a 50 fs time step, and were run for 3–5 μs. A simulation may be terminated if APS^{2-} reacts at the APS kinase site. The modeled APS^{2-} is flexible during the simulation, but their conformations do not vary significantly. As a result, we computed a distance between the central bead of APS^{2-} and the center-of-mass of its bound state in

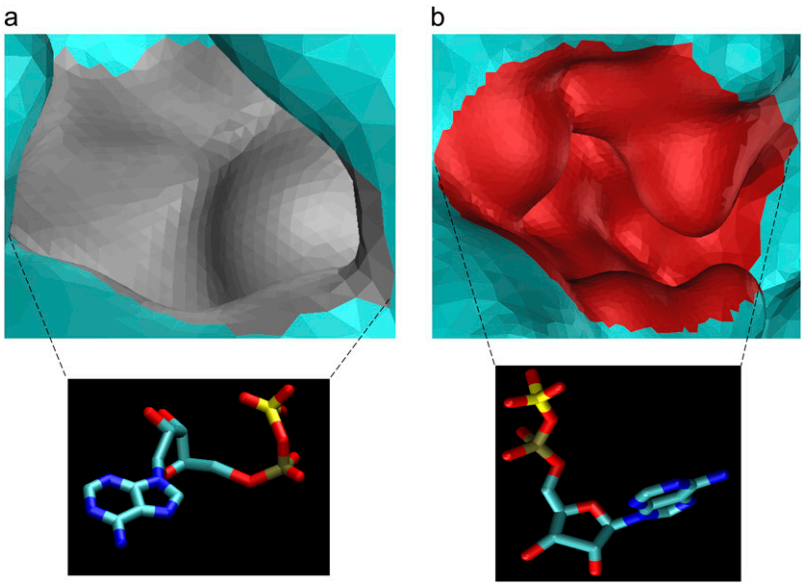

FIGURE 2 The active sites of ATP sulfurylase and APS kinase in the SAC dimer: (*a*) ATP sulfurylase; and (*b*) APS kinase.

the crystal structure to determine whether APS^{2-} is close to the APS kinase site. If the distance is <10 Å, then the APS^{2-} reacts at the APS kinase site. It is also assumed that APS^{2-} will not diffuse back to the protein and will be reduced by APS reductase in the solvent when it moves >50 Å away from the center-of-mass of the protein, thus a simulation may be stopped based on this criterion.

RESULTS AND DISCUSSIONS

Electrostatic steering in channeling

Before the channeling process simulation, the two reactive boundaries on the molecular surface of the SAC dimer need to be set up. Following Song et al. (25) and Tara et al. (41), each active site of ATP sulfurylase and APS kinase was based on multiple spheres placed on some atoms of the bound APS^{2-}. For the active site of ATP sulfurylase, three spheres, which are centered at N7 atom of the purine ring, $C3'$ of the ribose and the sulfur atom with 6, 8, and 6 Å radii, are placed on the APS^{2-} ligands in the crystal structure of the complex, respectively. For each active site of APS kinase, two spheres were centered at N1 atom of the purine ring and phosphorus atom with 8 Å and 9 Å radii, respectively. The actual reactive surface is then simply that portion of the new molecular surface due to the intersection of added spheres with molecule (Fig. 2).

The channeling process was first investigated with our steady-state Smoluchowski Solver (21). We have found that electrostatic steering is critical for channeling in the SAC dimer. Fig. 3 plots the calculated channeling efficiency (defined as the percentage of APS^{2-} that reaches the APS kinase active site via channeling rather than escaping into bulk solution) as a function of net charge of the APS^{2-} intermediate. At the experimental ionic strength ($\sim$40 mM), channeling efficiency is nearly 100% for the intermediate charge of $-2e$. Importantly, the channeling efficiency decreases to $<60\%$ for an uncharged intermediate. Our simulations suggest therefore that the high channeling efficiency observed experimentally does not result simply from the proximity of the two active sites: electrostatic effects appear necessary to account for efficient transfer (2,3,15,16). Our coarse-grained Brownian dynamics studies further demonstrated this fact. In our simulations, $>90\%$ of intermediates arrive at the APS kinase active site via channeling for $-2e$ charged intermediates. There is still $\sim$50% channeling even for the neutral case.

Comparing with the APS concentration distribution for different intermediate charges (Fig. 4), the average APS concentration in the solvent is nearly 400 times higher for the neutral APS^{0} than that for APS^{2-}. This fact indicates that electrostatic effects can constrain the APS^{2-} ions in the channel, which plays an essential role in efficient diffusion of APS between the two active sites.

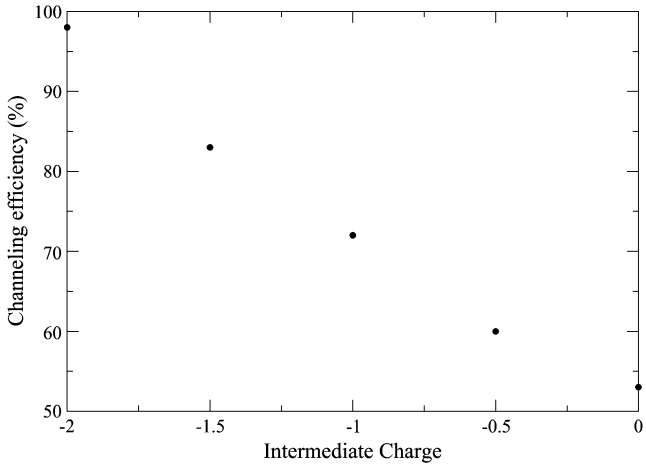

FIGURE 3 Dependence of channeling efficiency on the intermediate charge at 40 mM ionic strength.

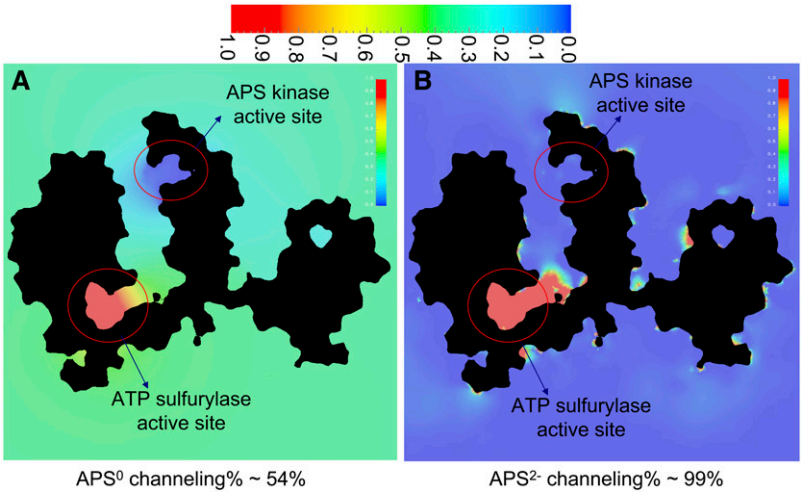

FIGURE 4 The intermediate concentration distribution in the solvent around SAC. Blue indicates extremely low concentration; cyan represents the medium low concentration and red the high concentration.

Furthermore, the time-dependent SMOL solver has been implemented to observe the channeling process along the simulation time (21). The influx of APS^{2-} in one active site of the APS kinase is shown in Fig. 5. It takes $\sim$1 μs for the whole system to reach the steady state, while the mean diffusion time for an APS^{2-} diffusion through the tunnel is $\sim$200 ns. The average concentration spilling out of the active site of ATP sulfurylase gradually increases to $\sim 10^{-9}$ nM to reach the steady state. Moreover, comparing with APS^0, the influx of APS^{2-} is three orders-of-magnitude higher, which substantially indicates the electrostatic steering during the channeling process.

Intermediate concentration distribution along the channel

To clearly depict the detailed intermediate distribution during the APS^{2-} channeling, the channel is divided evenly into 80 sections, 1 Å in length, along the line through the centers of the active sites of ATP sulfurylase and APS kinase (Fig. 6).

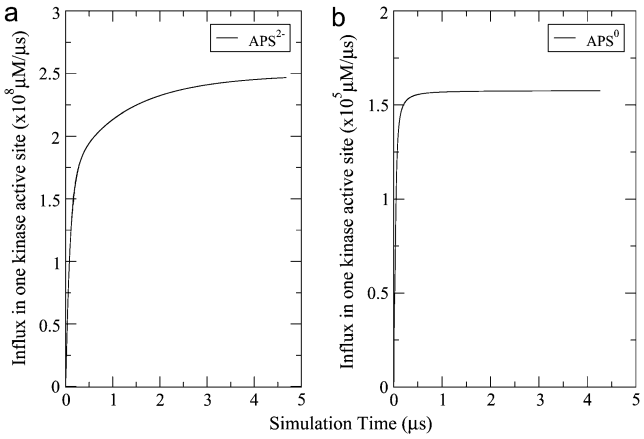

FIGURE 5 The influx of APS^{2-} and APS^0 in one active site of the APS kinase along the simulation time: (*a*) APS^{2-} and (*b*) APS^0.

The distribution probability of ions in each section for 78 independent CGBD simulations with different random seeds is plotted as shown in Fig. 7. The active site of the ATP sulfurylase is at zero distance. Three prominent peaks between the two active sites are observed in the histogram. The first peak is $\sim$10 Å away from the center of the active site of the ATP sulfurylase, while the other two peaks are $\sim$22 and 30 Å away. Between 35 Å and 45 Å axial distance, very few APS^{2-} ions are observed. Direct observation from the CGBD trajectories indicates that APS^{2-} ions do not smoothly flow into the APS kinase active site, but are absorbed abruptly. For example, during a 2 μs simulation, APS^{2-} ions spent $\sim$0.5 μs near the axial distance $\sim$30 Å, but they only spent $<$0.1 μs near the axial distance 40 Å. Furthermore, Fig. 8 draws the distribution of the center of APS^{2-} ion every 50 time steps. It must be noticed that most of the APS^{2-} ions during the channeling are accumulated in the areas around several α-helices, in which positively charged residues such as Lys^+ and Arg^+ are dominant. This observation also is consistent with the electrostatic potential distribution on the solvent-accessible surface (Fig. 9). The distribution of APS^{2-} along the channel reflects the positive electrostatic potential. This fact strongly supports the idea that APS^{2-} is transferred by electrostatically steered channeling. After the synthesis of APS^{2-} in the ATP sulfurylase active center, APS^{2-} diffuses into the channel due to the positive electrostatic potential at $\sim$10 Å axial distance. The APS^{2-} can accumulate between $\sim$20 and 35 Å axial distance and then moves abruptly through a somewhat less attractive region into the APS kinase active site. If the APS molecule is neutral, the APS^0 distribution in the channel is quite different (Fig. 10). There are more APS^0 molecules leaking into the solvent near the active site of ATP sulfurylase and very few entering into the active site of APS kinase.

The phosphorylation reaction in the APS kinase active site is nearly diffusion-controlled, while the synthesis of APS^{2-} is slower and essentially zero-order due to the relatively high concentrations of ATP^{4-} and SO_4^{2-}. Therefore, the

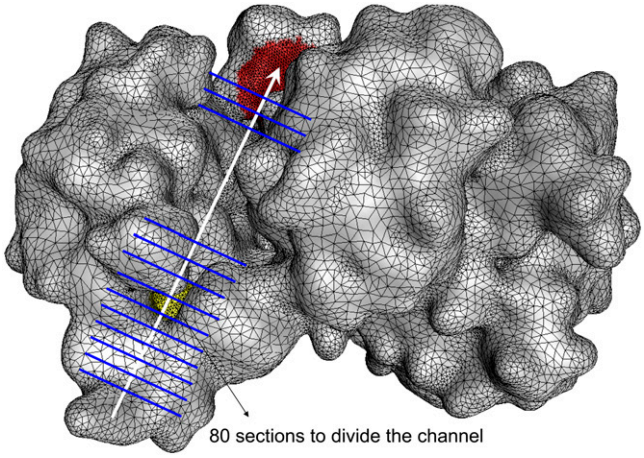

FIGURE 6 Eighty-one planes divide the channel into 80 sections through the active center of ATP sulfurylase to the active center of APS kinase. The average width of the channel is ~26 Å (20).

concentration of APS^{2-} in the channel should not be negligible. By solving the time-dependent Smoluchowski equation, the distribution probability of APS^{2-} is also plotted for different simulation times (Fig. 11). Similarly with our CGBD results, two relatively prominent peaks are observed between 20 and 35 Å axial distance. The first peak corresponding to the CGBD simulation is not differentiated because continuum modeling describes the cumulative effect of APS^{2-} channeling, while CGBD only describes the pathway of one single APS^{2-}. Interestingly, the relative height of the peaks between the two active sites is similar for both the continuum modeling and CGBD simulations. It is worth noting that our coarse-grained model does not have explicit water molecules, so the model may not accurately represent

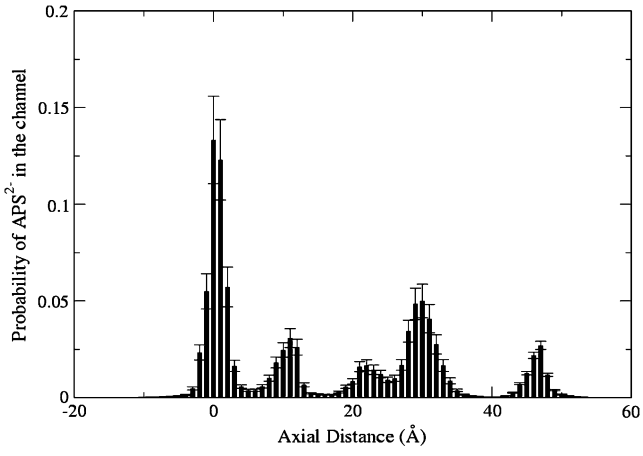

FIGURE 7 A dwell histogram indicates the region of the channel where APS^{2-} ions preferentially reside. The channel is divided into 80 sections, and the average probability in each slice is counted during 78 independent CGBD simulations of 2 μs. The standard deviation is represented with the line.

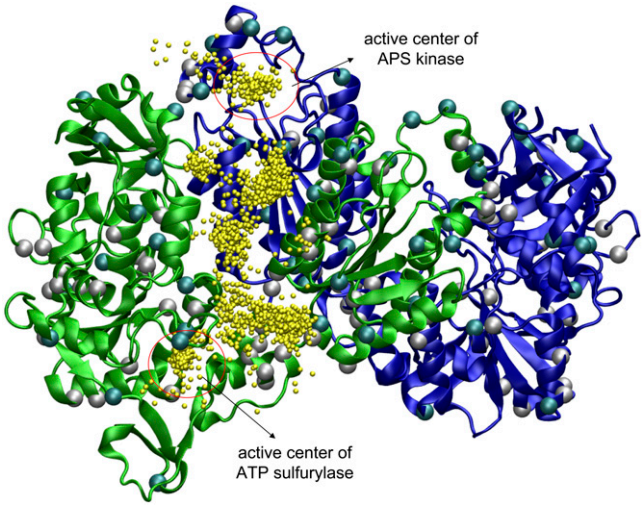

FIGURE 8 The APS^{2-} distribution in the channel in one of CGBD simulations. The blue represents one monomer and the green the other monomer. The yellow represents where the center of APS^{2-} resides in 2 μs simulation. The cyan and white spheres represent Lys^{+} and Arg^{+}, respectively.

the desolvation penalty. For systems that have tightly bound waters, our current model may need modifications to capture the solvent effects more accurately.

We also studied the neutral APS^{0} in CGBD simulations; as in the continuum modeling, the distribution of APS has substantial changes from that of APS^{2-} (Fig. 12). There are more APS^{0} molecules diffusing toward the solvent rather than the channel. For those in the channel, very few can enter the APS kinase active site. Therefore, no APS peak is shown corresponding to the APS kinase active site.

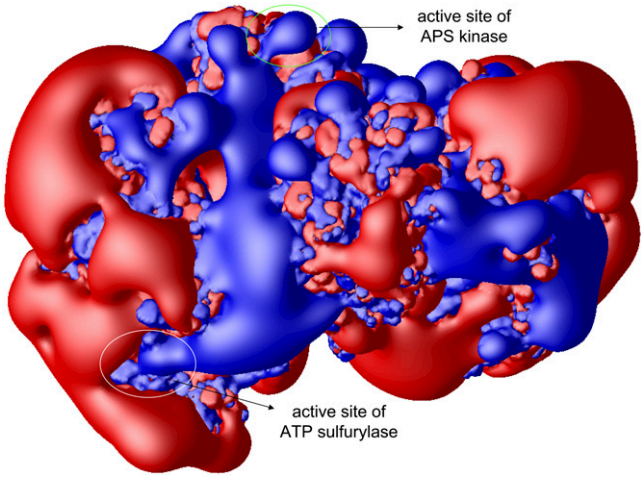

FIGURE 9 The electrostatic potential on the surface of the SAC complex. The red and blue represent the negative and positive potentials larger than 1 kT/e, respectively.

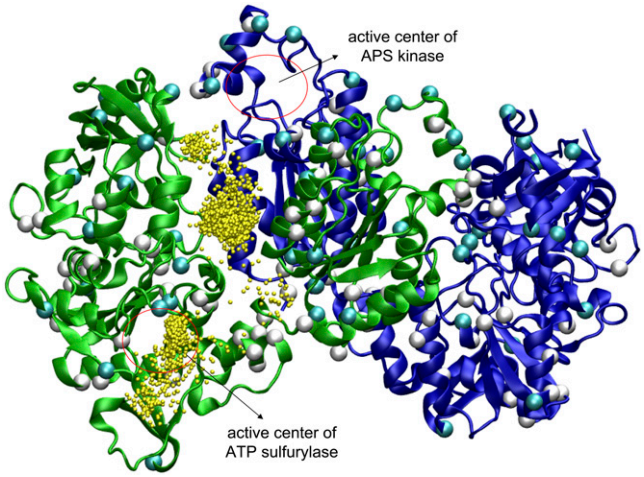

FIGURE 10 The APS^0 distribution in the channel in one of CGBD simulations. The blue represents one monomer and the green the other monomer. The yellow represents where the center of APS^{2-} resides in 2 μs simulation. The cyan and white spheres represent Lys^+ and Arg^+, respectively.

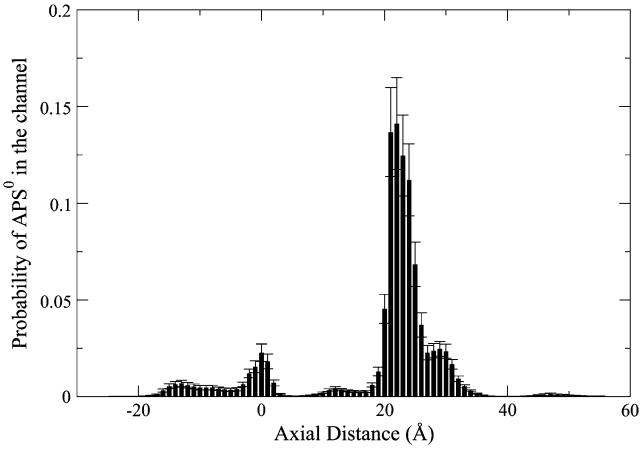

FIGURE 12 A dwell histogram indicates the region of the channel where the neutral ligands preferentially reside. The channel is divided into 80 sections, and the average probability in each slice is counted during 69 independent CGBD simulations of 2 μs. The standard deviation is represented with the line.

CONCLUSION

In this study we have elucidated the channeling behavior of the intermediate APS^{2-} in the type III SAC complex using both the continuum modeling and coarse-grained Brownian dynamics approaches, thus gaining insight into the channeling mechanism at the continuous and discrete levels.

First, by solving the steady-state Smoluchowski equation, the channeling efficiency is observed to substantially depend on the net charge of the intermediate. Increasing the net charge causes weakened interaction between the APS^{2-} and SAC complex and as a consequence, reduces APS channeling efficiency (Fig. 3). The simulations suggest that there is only ~50% transferring through channeling for the neutral intermediate, while nearly 99% for the APS^{2-}. This result is consistent with the previous experimental studies, which show $\geqq$95% channeling in the type III complex (20). Moreover, the APS^{2-} and APS^0 influx of the APS kinase active site has been compared by solving the time-dependent Smoluchowski equation. This indicates that the influx of APS^0 is three orders-of-magnitude lower than that of APS^{2-} (Fig. 5).

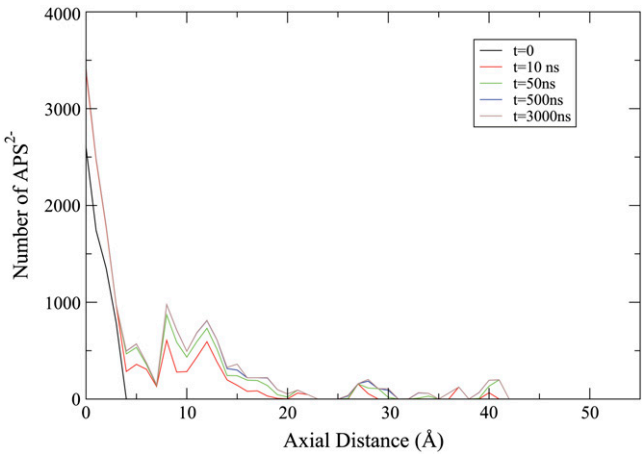

FIGURE 11 The APS^{2-} axial distribution during the channeling process simulated with the SMOL solver. In each section, only the APS^{2-} ions within 15 Å from the axis were counted. When t = 0, 10, 50, 500, and 3000 ns, there are 39,497, 72,695, 75,611, 77,031, and 77,178 APS^{2-} ions released from one ATP sulfurylase active site.

Second, we have explored the detailed channeling profile with the CGBD. The results are consistent with our continuum simulations. Furthermore, the CGBD results imply that the positively charged residues along the channel might play an important role in guiding the APS^{2-} into the active center of the APS kinase. The distribution of APS^{2-} is relatively more averaged in the channel than the distribution of APS^0. It must be noted that the APS^0 can seldom enter the active site of the APS kinase, which indicates that the positive residues such as Lys^+ and Arg^+ around the APS kinase active site are essential for the phosphorylation reaction (Eq. 2). In addition, it must be noted that there are at least 14 residues carrying positive charges around the active pocket of the APS kinase (Fig. 8 or 10). Any mutation to the neutral residues might affect the APS^{2-} channeling efficiency.

By comparing with the previous computational studies on the DHFR-TS (16), we have observed a similar phenomenon in this type III SAC complex. Our theoretical studies demonstrate that the APS^{2-} may be channeled across the ''electrostatic highway'' between the two active sites of the ATP sulfurylase and APS kinase in the type III SAC complex (42). The electrostatic interaction between the intermediate and the SAC not only restricts the intermediate to the channel, but decreases the channeling barrier. Furthermore, the electrostatic interaction guiding the intermediate into the APS kinase active site perhaps enhances the catalytic efficiency of the phosphorylation of APS^{2-}. In addition, this study did not

include the slower protein fluctuations, although, according to the experiment in Sun and Leyh (20), ''open'' and ''closed'' states exist. Our future work will try to clarify the relationship between the protein conformations and the kinetics of the APS intermediate (43,44).

We thank Jane Ren for assistance in developing the SMOL code for this study. We also thank Yongcheng Zhou for help with numerical simulations.

Funding by National Institutes of Health grant No. GM31749 and National Science Foundation grants No. MCB-0506593 and MCA93S013 (to J.A.M.) supported this work. Additional support from the Howard Hughes Medical Institute, the National Science Foundation Supercomputer Centers, the San Diego Supercomputing Center, Accelrys, Inc., the W.M. Keck Foundation, the National Biomedical Computational Resource, and the Center for Theoretical Biological Physics is gratefully acknowledged.

REFERENCES

1. Huang, X. Y., H. M. Holden, and F. M. Raushel. 2001. Channeling of substrates and intermediates in enzyme-catalyzed reactions. *Annu. Rev. Biochem.* 70:149–180.
2. Miles, E. W., S. Rhee, and D. R. Davies. 1999. The molecular basis of substrate channeling. *J. Biol. Chem.* 274:12193–12196.
3. Elcock, A. H. 2002. Atomistic simulations of competition between substrates binding to an enzyme. *Biophys. J.* 82:2326–2332.
4. Ushiroyama, T., T. Fukushima, J. D. Styre, and H. O. Spivey. 1992. Substrate channeling of NADH in mitochondrial redox processes. *Curr. Top. Cell. Regul.* 33:291–307.
5. Rudolph, J., and J. Stubbe. 1995. Investigation of the mechanism of phosphoribosylamine transfer from glutamine phosphoribosylpyrophosphate amidotransferase to glycinamide ribonucleotide synthetase. *Biochemistry.* 34:2241–2250.
6. Atkinson, D. E. 1969. Regulation of enzyme function. *Annu. Rev. Microbiol.* 23:47–68.
7. Dewar, M. J. S., and D. M. Storch. 1985. Alternative view of enzyme-reactions. *Proc. Natl. Acad. Sci. USA.* 82:2225–2229.
8. Easterby, J. S. 1981. A generalized theory of the transition time for sequential enzyme-reactions. *Biochem. J.* 199:155–161.
9. Kholodenko, B. N., O. V. Demin, and H. V. Westerhoff. 1993. Channeled pathways can be more sensitive to specific regulatory signals. *FEBS Lett.* 320:75–78.
10. Reddy, G. P. V., and A. B. Pardee. 1980. Multi-enzyme complex for metabolic channeling in mammalian DNA-replication. *Proc. Natl. Acad. Sci. USA.* 77:3312–3316.
11. Edwards, M. R. 1996. Metabolite channeling in the origin of life. *J. Theor. Biol.* 179:313–322.
12. Petrushenko, Z. M., T. V. Budkevich, V. F. Shalak, B. S. Negrutskii, and A. V. El'skaya. 2002. Novel complexes of mammalian translation elongation factor eEF1A·GDP with uncharged tRNA and aminoacyl-tRNA synthetase—implications for tRNA channeling. *Eur. J. Biochem.* 269:4811–4818.
13. Johnson, J. L., J. K. West, A. D. L. Nelson, and G. D. Reinhart. 2007. Resolving the fluorescence response of *Escherichia coli* carbamoyl phosphate synthetase: mapping intra- and intersubunit conformational changes. *Biochemistry.* 46:387–397.
14. Anderson, A. C. 2005. Two crystal structures of dihydrofolate reductase-thymidylate synthase from *Cryptosporidium hominis* reveal protein-ligand interactions including a structural basis for observed antifolate resistance. *Acta Crystallogr. F Struct. Biol. Cryst. Commun.* 61:258–262.
15. Elcock, A. H., M. J. Potter, D. A. Matthews, D. R. Knighton, and J. A. McCammon. 1996. Electrostatic channeling in the bifunctional enzyme dihydrofolate reductase-thymidylate synthase. *J. Mol. Biol.* 262:370–374.
16. Elcock, A. H., and J. A. McCammon. 1996. Evidence for electrostatic channeling in a fusion protein of malate dehydrogenase and citrate synthase. *Biochemistry.* 35:12652–12658.
17. Amaro, R., and Z. Luthey-Schulten. 2004. Molecular dynamics simulations of substrate channeling through an α-β barrel protein. *Chem. Phys.* 307:147–155.
18. Floquet, N., S. Mouilleron, R. Daher, B. Maigret, B. Badet, and M. A. Badet-Denisot. 2007. Ammonia channeling in bacterial glucosamine-6-phosphate synthase (GLMS): molecular dynamics simulations and kinetic studies of protein mutants. *FEBS Lett.* 581:2981–2987.
19. Sun, M. H., J. L. Andreassi, S. Q. Liu, R. Pinto, J. A. Triccas, and T. S. Leyh. 2005. The trifunctional sulfate-activating complex (SAC) of mycobacterium tuberculosis. *J. Biol. Chem.* 280:7861–7866.
20. Sun, M. H., and T. S. Leyh. 2006. Channeling in sulfate activating complexes. *Biochemistry.* 45:11304–11311.
21. Cheng, Y. H., J. K. Suen, Z. Radić, S. D. Bond, M. J. Holst, and J. A. McCammon. 2007. Continuum simulations of acetylcholine diffusion with reaction-determined boundaries in neuromuscular junction models. *Biophys. Chem.* 127:129–139.
22. Holst, M., N. Baker, and F. Wang. 2000. Adaptive multilevel finite element solution of the Poisson-Boltzmann equation. I. Algorithms and examples. *J. Comput. Chem.* 21:1319–1342.
23. Baker, N., M. Holst, and F. Wang. 2000. Adaptive multilevel finite element solution of the Poisson-Boltzmann equation. II. Refinement at solvent-accessible surfaces in biomolecular systems. *J. Comput. Chem.* 21:1343–1352.
24. Baker, N. A., D. Sept, S. Joseph, M. J. Holst, and J. A. McCammon. 2001. Electrostatics of nanosystems: application to microtubules and the ribosome. *Proc. Natl. Acad. Sci. USA.* 98:10037–10041.
25. Song, Y. H., Y. J. Zhang, C. L. Bajaj, and N. A. Baker. 2004. Continuum diffusion reaction rate calculations of wild-type and mutant mouse acetylcholinesterase: adaptive finite element analysis. *Biophys. J.* 87:1558–1566.
26. Song, Y. H., Y. J. Zhang, T. Y. Shen, C. L. Bajaj, J. A. McCammon, and N. A. Baker. 2004. Finite element solution of the steady-state Smoluchowski equation for rate constant calculations. *Biophys. J.* 86: 2017–2029.
27. Yu, Z., M. Holst, Y. Cheng, and J. A. McCammon. 2008. Feature-preserving adaptive mesh generation for molecular modeling. *J. Mol. Graph. Model.* 26:1370–1380.
28. Zhang, D. Q., J. Suen, Y. J. Zhang, Y. H. Song, Z. Radić, P. Taylor, M. J. Holst, C. Bajaj, N. A. Baker, and J. A. McCammon. 2005. Tetrameric mouse acetylcholinesterase: continuum diffusion rate calculations by solving the steady-state Smoluchowski equation using finite element methods. *Biophys. J.* 88:1659–1665.
29. Mackay, R. S., and D. J. C. Mackay. 2006. Ergodic pumping: a mechanism to drive biomolecular conformation changes. *Physica D.* 216:220–234.
30. Cheng, Y. H., J. K. Suen, D. Q. Zhang, S. D. Bond, Y. J. Zhang, Y. H. Song, N. A. Baker, C. L. Bajaj, M. J. Holst, and J. A. McCammon. 2007. Finite element analysis of the time-dependent Smoluchowski equation for acetylcholinesterase reaction rate calculations. *Biophys. J.* 92:3397–3406.
31. Tozzini, V., and J. A. McCammon. 2005. A coarse grained model for the dynamics of flap opening in HIV-1 protease. *Chem. Phys. Lett.* 413:123–128.
32. Chang, C. E., T. Shen, J. Trylska, V. Tozzini, and J. A. McCammon. 2006. Gated binding of ligands to HIV-1 protease: Brownian dynamics simulations in a coarse-grained model. *Biophys. J.* 90:3880–3885.
33. Tozzini, V., J. Trylska, C. E. Chang, and J. A. McCammon. 2007. Flap opening dynamics in HIV-1 protease explored with a coarse-grained model. *J. Struct. Biol.* 157:606–615.
34. Scott, E. E., Q. H. Gibson, and J. S. Olson. 2001. Mapping the pathways for O_2 entry into and exit from myoglobin. *J. Biol. Chem.* 276:5177–5188.
35. Ermak, D. L., and J. A. McCammon. 1978. Brownian dynamics with hydrodynamic interactions. *J. Chem. Phys.* 69:1352–1360.

36. Shen, T. Y., C. F. Wong, and J. A. McCammon. 2001. Atomistic Brownian dynamics simulation of peptide phosphorylation. *J. Am. Chem. Soc.* 123:9107–9111.

37. Panchenko, A. R., J. Wang, G. U. Nienhaus, and P. G. Wolynes. 1995. Analysis of ligand-binding to heme-proteins using a fluctuating path description. *J. Phys. Chem.* 99:9278–9282.

38. Wang, J., and P. Wolynes. 1995. Intermittency of single-molecule reaction dynamics in fluctuating environments. *Phys. Rev. Lett.* 74: 4317–4320.

39. Mazur, J., and R. L. Jernigan. 1991. Distance-dependent dielectric-constants and their application to double-helical DNA. *Biopolymers.* 31:1615–1629.

40. Vasilyev, V. 2002. Determination of the effective dielectric constant from the accurate solution of the Poisson equation. *J. Comput. Chem.* 23:1254–1265.

41. Tara, S., A. H. Elcock, J. M. Briggs, Z. Radić, P. Taylor, and J. A. McCammon. 1998. Rapid binding of a cationic active site inhibitor to wild type and mutant mouse acetylcholinesterase: Brownian dynamics simulation including diffusion in the active site gorge. *Biopolymers.* 46:465–474.

42. Stroud, R. M. 1994. An electrostatic highway. *Nat. Struct. Biol.* 1:131–134.

43. Zhou, Y. Q., C. Zhang, G. Stell, and J. Wang. 2003. Temperature dependence of the distribution of the first passage time: results from discontinuous molecular dynamics simulations of an all-atom model of the second β-hairpin fragment of protein G. *J. Am. Chem. Soc.* 125: 6300–6305.

44. Lee, C. L., C. T. Lin, G. Stell, and J. Wang. 2003. Diffusion dynamics, moments, and distribution of first-passage time on the protein-folding energy landscape, with applications to single molecules. *Phys. Rev. E Stat. Nonlin. Soft Matter Phys.* 67:066307.